Astronomy & Astrophysics manuscript no. Didymos_Opitom_corr
March 6, 2023

Letter to the Editor

Morphology and spectral properties of the DART impact ejecta with VLT/MUSE

C. Opitom[1], B. Murphy[1], C. Snodgrass[1], S. Bagnulo[2], S. F. Green[3], M. M. Knight[4], J. de Léon[5,6], J.-Y. Li[7], and D. Gardener[1]

[1] Institute for Astronomy, University of Edinburgh, Royal Observatory, Edinburgh EH9 3HJ, UK
e-mail: copi@roe.ac.uk
[2] Armagh Observatory & Planetarium, College Hill, Armagh, BT61 9DG, UK
[3] School of Physical Sciences, The Open University, Milton Keynes MK7 6AA, UK
[4] United States Naval Academy, Annapolis, MD, USA
[5] Instituto de Astrofísica de Canarias (IAC), C/Vía Láctea s/n, E-38205 La Laguna, Spain
[6] Department of Astrophysics, University of La Laguna, Tenerife, Spain
[7] Planetary Science Institute, Tucson, AZ, USA

ABSTRACT

Context. On September 26, 2022, the NASA DART mission impacted the asteroid Dimorphos, the smaller component of the Didymos binary asteroid system. This provided a unique opportunity to observe, in real time, the evolution of the ejecta cloud produced by the impact and the formation of a tail.
Aims. We present observations performed with the MUSE instrument at the Very Large Telescope to characterise the morphology, spectral properties, and evolution of the ejecta. The Didymos system was observed with MUSE on 11 nights from just before impact to almost one month post-impact, using both wide-field observations without adaptive optics and narrow-field observations with adaptive optics.
Methods. We produced white light images that were used to study the morphology of the ejecta at different spatial scales. The spectral information was used to search for gas emission from either exposed ice or propellant, and to study the spatial and temporal variation of the ejecta dust reflectance through reflectance maps.
Results. We searched for, but did not detect, emission from [OI], Xe, NH_2, and H_2O^+ in a $1'\times1'$ field of view in our observations starting almost 4h after impact. We detected a number of morphological features, including a short-lived ejecta cloud visible on September 27 towards the east, spirals, clumps, and a tail that started forming only a few hours after impact. The analysis of the reflectance maps showed that the initial ejecta was bluer than the system before impact, while the tail and spirals were redder than the initial ejecta, consistent with them being made of larger particles. Over the few weeks following impact, the tail became redder. No significant colour differences could be seen between the clumps and the initial ejecta.

1. Introduction

The Double Asteroid Redirection Test (DART) NASA mission is the first planetary defence mission aimed at testing asteroid deflection through impact (Rivkin et al. 2021). The mission targeted the Didymos binary system, which is composed of the 761 m diameter asteroid Didymos and the much smaller moon Dimorphos (151 m) (Daly et al. 2023). DART impacted Dimorphos on 26 September 2022 at 23:14 UT. Even though evidence shows that asteroid impacts occur regularly, they cannot be predicted in advance. The DART mission provided a unique opportunity to study an asteroid impact in real time, and the morphological and spectroscopic properties of the ejecta cloud it produced. The DART spacecraft was destroyed on impact, but the LICIACube cubesat (Dotto et al. 2021), released from DART about two weeks before impact, provided very high resolution images of the initial ejecta on a short timescale, in the few minutes following the impact. The assessment of the effect of the impact over timescales of hours to weeks was achieved through ground- and space-based support observations (see e.g. Thomas et al. 2023; Li et al. 2023). In this manuscript, we report observations of the impact ejecta over a month using the Very Large Telescope (VLT) Unit Telescope 4 Multi Unit Spectroscopic Explorer (MUSE) instrument. These observations allowed us to simultaneously study and establish correlations between the morphology and spectral properties of the ejecta, with a subarcsecond spatial resolution. They were part of a coordinated campaign using all four VLTs to simultaneously study the impact and evolution of the ejecta in a synergistic manner.

2. Observations and data reduction

We observed the Didymos–Dimorphos system with the MUSE instrument on the VLT in combination with the Adaptive Optics Facility (Arsenault et al. 2008; Ströbele et al. 2012), from just before the impact to about a month after impact. MUSE is an integral field spectrograph (IFU) covering the full visible range

Table 1. Observing circumstances of the 2I VLT campaign

Date	Time (UT)	Instrument Set-up	N	ΔT (h)	α (deg)	Δ (au)	Scale (km)
2022-09-26	07:51-09:08	NFM+WFM	6+4	-15	52.3	0.0765	55.45
2022-09-27	02:55-08:02	NFM+WFM	8+15	+6	53.6	0.0754	54.72
2022-09-28	03:54-08:17	NFN+WFM	6+14	+31	55.2	0.0743	53.90
2022-09-29	06:10-09:07	NFM+WFM	5+5	+56	56.7	0.0734	53.21
2022-10-01	06:30-09:08	NFM+WFM	5+4	+107	59.7	0.0720	52.21
2022-10-03	07:22-09:09	WFM	10	+153	62.7	0.0713	51.73
2022-10-04	06:19-07:52	WFM	8	+176	64.0	0.0712	51.66
2022-10-07	05:51-09:31	NFM+WFM	4+10	+248	67.9	0.0719	52.12
2022-10-14	05:42-08:50	WFM	24	+416	74.2	0.0781	56.64
2022-10-19	05:31-08:59	WFM	25	+536	76.1	0.0857	62.14
2022-10-25	05:52-08:56	WFM	24	+680	76.0	0.0969	70.30

Notes. N represents the number of exposures obtained, ΔT the number of hours between impact and the observations mid-point, α the Sun-comet-Earth phase angle, Δ the geocentric distance, and scale the number of kilometres covered by 1″ at the geocentric distance of the system.

(from 480 to 920 nm), with a spectral resolving power of about 3000 (Bacon et al. 2010). We used the instrument in two different modes: the Narrow Field Mode (NFM) with adaptive optics and an 8″×8″ field of view (FoV) and the Wide Field Mode (WFM) without adaptive optics and a 1′×1′ FoV. We used exposure times ranging from 300 to 600 s, depending on the brightness of the object and how crowded the background field was. A summary of the data obtained is presented in Table 1.

For each mode the observing sequences consisted of several exposures centred on Didymos, with dither and 90-degree rotation between exposures, to allow correction of detector-to-detector effects. Two exposures of the sky, between 5 and 10′ from the system, were obtained for each sequence as we expected the ejecta to fill the MUSE field, particularly in NFM. For the later observing dates an offset (and rotation) was applied to some observations to place the system at the edge of the field and sample a larger part of the tail. The data were reduced using the MUSE pipeline (Weilbacher et al. 2020), including flux calibration and telluric correction using the spectrophotometric standard star observed during each night. For the WFM data we tested background subtraction using dedicated sky exposures and part of the science exposure without signal from the object. We found that using areas of the science exposures led to lower sky residuals, and we used it for all WFM data. For NFM data, as the ejecta filled most of the FoV, we used the dedicated sky exposures to subtract the background.

3. Results and discussion

3.1. Presence of gas

We searched our datacubes for gas emission, resulting either from exposed ice uncovered by the impact or from the vaporisation of the propellants contained within the DART spacecraft itself. There are several well-known emission lines and/or bands within the MUSE wavelength range, but we focused our search on four species. Given that our first observations were obtained over 3h after impact, we used WFM data with a larger FoV to search for gas emission. Gas moving at a velocity of 1 km/s (typical for gas produced by sublimation at 1 au from the Sun) travels 14,400 km in 4h, which is over a factor of 4 more than what is covered by our field. This means that the component of any gas emitted at impact along the plane of sky will likely be outside our FoV. However, gas expanding in other directions will have a lower projected velocity and might still be detected if present in sufficient amounts.

3.1.1. Gas from exposed ice or refractory material

[OI] forbidden emission lines around 558, 630, and 636 nm result from the dissociation of water (or other oxygen-bearing molecules). These lines could have been detected if sub-surface water ice had been present within Dimorphos and was exposed by the impact. We focused on the brightest of the three lines at 630 nm, following the procedure described in Opitom et al. (2020). At the resolving power of MUSE, the [OI] 630 nm line is blended with a telluric line. In datacubes without sky subtraction applied, we mapped the intensity of the [OI] line across the MUSE FoV, looking for intensity enhancement associated with emission coming from the ejecta. Because the emission from the object would coincide with a variable telluric line, we could only detect variations in the [OI] intensity of the order of 3×10^{-18} $erg/cm^2/s$ over the 1′×1′ FoV of MUSE in a single observation 4h after impact. Any emission homogeneous across the field cannot be distinguished from sky signatures. We also looked for traces of H_2O^+ that would be produced by the ionisation of water. In this case, after subtracting the continuum contribution for each spaxel of the datacubes, we produced maps of the intensity around the wavelength of the H_2O^+ (8,0) band around 620 nm. No sign of H_2O^+ was detected in the data from the night directly after impact. Based on the standard deviation of the values in our maps, we would have been able to detect a flux of the order of 2×10^{-18} $erg/cm^2/s$ for H_2O^+ in a 5″×5″ aperture in a single observation 4h after impact. Finally, we also looked for Na emission, but due to a strong telluric emission of sodium on the night after impact, we could not perform a sensitive search for sodium.

3.1.2. Gas from propellant

Discussions within the DART science team following the observations of a fast plume in the minutes following the impact considered whether it could have been driven by leftover fuel expelled from the spacecraft during impact. The DART spacecraft contained hydrazine as propellant. Hydrazine (N_2H_4) photodissociates into NH_3 (Stief et al. 2020), which then dissociates into NH_2. NH_2 has several emission bands in the MUSE wavelength range. Around 1 au, NH_3 has a lifetime of about a few hours and NH_2 of more than 20 h, meaning that if present in sufficient

amounts, hydrazine photodissociation products could have been detected around Didymos even several hours after impact. Using the continuum-subtracted data, we extracted the cubes around the wavelengths of the brightest part of the NH_2 A-X (0,4,0)-(0,0,0), and A-X (0,3,0)-(0,0,0) bands. We did not find traces of NH_2 emission in individual maps or after combining maps observed between 02:55 and 08:02 UT on September 27.

Finally, we looked for emission from xenon. The DART spacecraft contained Xe used by the ion engine. There are several bright Xe lines in the MUSE wavelength range, in particular at 823 and 828 nm. Following the same methodology as for NH_2 and H_2O^+, we produced maps of Xe using the MUSE WFM observations of September 27. No signal was detected in these maps. Based on the standard deviation of the values in our maps, we would have been able to detect a flux of the order of 9×10^{-18} and 6×10^{-18} $erg/cm^2/s$ for NH_2 and Xe respectively in a 5″×5″ aperture in single observations 4h after impact.

In addition to the methods mentioned above, we also searched for emission lines in spectra extracted around the system. This is illustrated in the upper panel of Figure 1, showing a spectrum extracted within a 5″ radius aperture on September 27. This spectrum shows the lack of clear emission lines or bands following the impact. Given the lack of spherical symmetry and the unsteady state of the system, defining upper limits of the production rates of the various species based on our data would require dedicated modelling that is beyond the scope of this paper; standard cometary techniques cannot be used in this case.

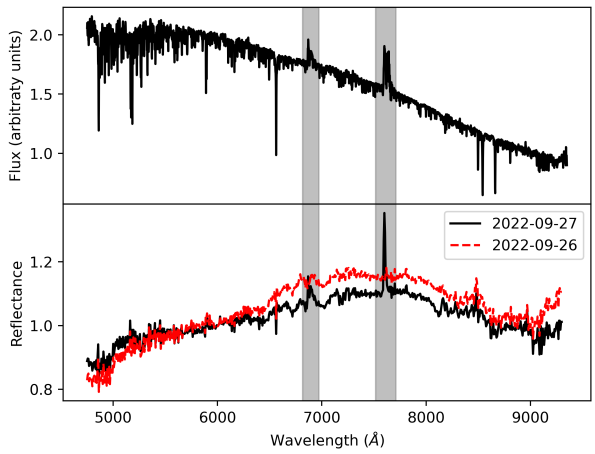

Fig. 1. Spectrum of Didymos over the MUSE wavelength range. Upper: Spectrum of Didymos measured within a 5″ radius aperture on September 27, illustrating the absence of emission lines following the impact. Lower: Reflectance of Didymos on the same date computed using a solar spectrum and a factor of 5 binning in the spectral direction. Overplotted in red for comparison is the reflectance spectrum of Didymos on September 26, pre-impact. Grey areas are strongly affected by telluric absorption.

3.2. Morphology of the ejecta

From our datacubes, we produced a series of white light images for each of the exposures listed in Table 1. The collapsed 2D images maintained the spatial resolution of the original datacubes and the original plate scales of 0.2″/pix for MUSE WFM and 0.025″/pix for MUSE NFM. We analysed the morphological evolution of the ejecta in the WFM and NFM images, specifically tracking early clumps (concentrations of material with no resolvable structure) in the ejecta plume. We sought to increase the signal-to-noise ratio in our observations while preserving high temporal resolution, so we co-added exposures in one-hour blocks in both modes for the first two nights, and for the whole sequence for the nights after that. We created and analysed a total of 21 stacked images for WFM and 7 for NFM, which allowed us to probe two unique spatial regimes for several weeks after impact.

Similarly to what was observed with the Hubble Space Telescope (HST; Li et al. 2023), a few hours after impact we saw extensive amounts of ejected material around the Didymos–Dimorphos system in an eastern-facing cone, visible in our first observations starting at 02:55 UT September 27. This ejecta displayed many smaller structures moving radially outwards, indicating they are fast moving and have likely not been significantly affected by the gravity of the binary or radiation pressure (Li et al. 2023). Several of these clumps of material are outlined in panels (a) to (c) of Figure 2. Several hours after impact, the effect of radiation pressure pushing dust particles in the anti-sunward direction becomes visible. A tail has formed and can be seen in our NFM and WFM observations obtained around 07:00 UT on September 27 (panel (c)). Over the next days to weeks, the tail expands as small particles are pushed further and eventually leave our FoV, while larger particle move on longer timescales. Consistent with HST observations by Li et al. 2023, by September 28 (panel (d)), curved features (referred to as spirals and indicated by green arrows in panel (e) of Figure 2) have appeared: one located to the north and another to the southeast. The curvature of these features can be seen more clearly in NFM observations of September 28 and October 1 (panels (d) and (e)), which have a spatial resolution comparable to HST. Li et al. 2023 postulate that these features are composed of slower dust particles which have interacted gravitationally with the binary system, distorting the original ejecta cone to produce curved features. Over time, the southern spiral splits into several linear features visible in the NFM data of October 1 and in the WFM data of October 7 due to the effect of the radiation pressure. The radiation pressure also causes the northern spiral to broaden, as smaller particles are pushed further than larger ones, and later detach from the system entirely, as illustrated in the NFM data in panel (e) and the WFM data in panel (f). Finally, we note the double tail visible on October 14 (panel (g)), whose origin is still unclear.

Estimated plane of sky expansion velocities were derived for a set of notable clumps seen in panels (a) to (c) of Figure 2 and located at similar projected distances from the system. These clumps are marked by ellipses in panels (a) to (c) of Figure 2. All clumps appear to be moving at a similar projected velocity of $\bar{v}_{\rm clumps} = 13.7 \pm 2$ m s^{-1} (average of the velocity measured for the three clumps). Taking into account the projected velocity and the time at which the positions of the clumps were measured, this is consistent with an ejection around the time of impact. This velocity is also consistent with the values for the motion of similar features seen in HST images (Li et al. 2023).

3.3. Spectral properties of the ejecta

We took advantage of the IFU nature of MUSE to study the spatial variation in the dust spectral properties across the ejecta. In particular, we focused on the relative spectral reflectance and its slope. The relative spectral reflectance is obtained by dividing the spectrum of the object by the solar spectrum. We focused

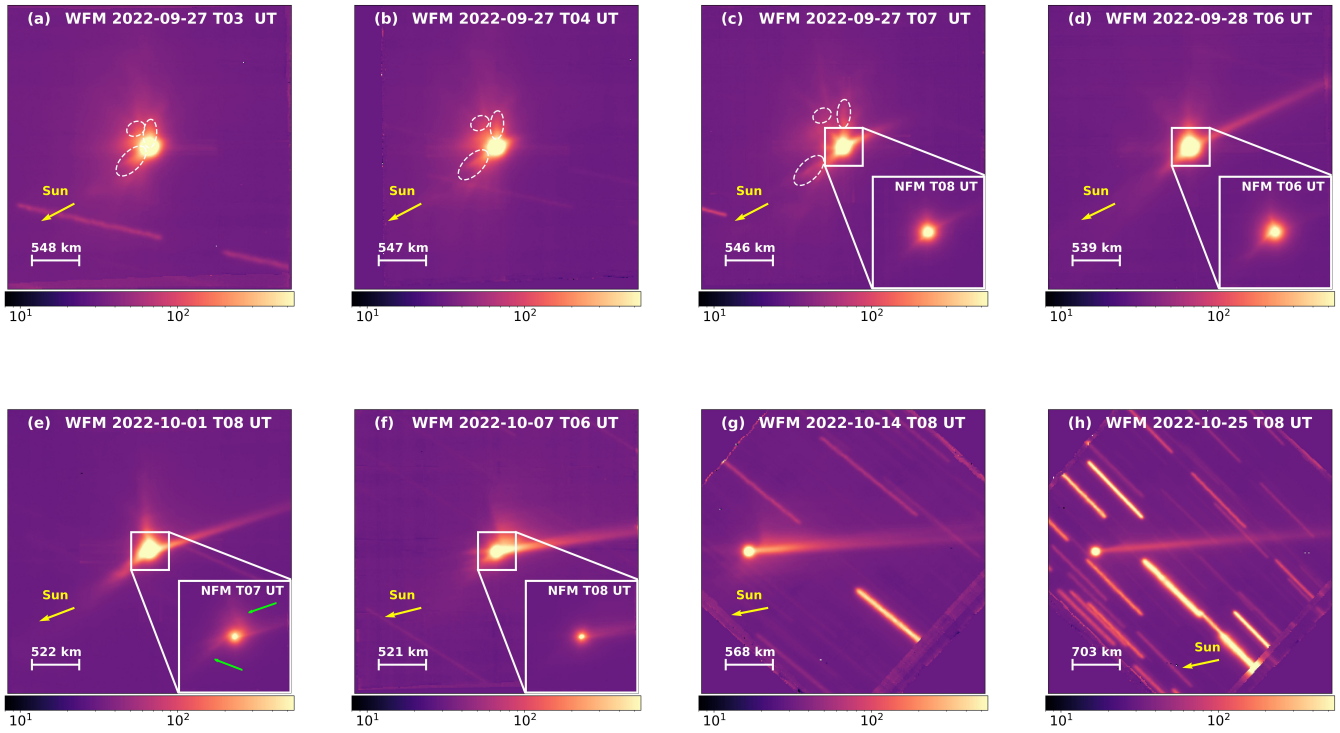

Fig. 2. Evolution of the ejecta morphology seen from white light images in WFM at different dates. Panels (c) to (f) include insets showing almost simultaneous images in NFM using adaptive optics. All images are oriented north up and east left. Intensities are in units of 10^{-20} erg/s/cm^2. The ellipses indicate the position of the clumps referred to in the text. The green arrows indicate the spirals mentioned in the text. The direction of the Sun and a scale bar are shown in each panel.

our analysis on the WFM data, while the NFM reflectance map will be discussed in detail in a follow-up publication.

The relative reflectance measured in a 5″ aperture on September 27 increases with wavelength between 480 and 750 nm, and then decreases slowly between 750 and 900 nm, (Figure 1). Its shape is consistent with the reflectance spectrum measured pre-impact with MUSE and what is measured with other instruments. More details on the measurement of the reflectance can be found in Appendix A.

For each datacube we computed the relative reflectance spectrum normalised at 600 nm for each spaxel individually. We fitted a slope (first-order polynomial) to the relative reflectance between 500 and 750 nm (to match the cut-off wavelength to the peak of the reflectance) and produced a map with the value of this slope for each spaxel of each datacube. A signal cut-off was applied to mask the spaxels with little to no comet signal. We then re-centred and median-combined maps of the reflectance slope for each observing night to increase the signal-to-noise ratio and attenuate detector-to-detector effects (exposures strongly contaminated by star trails were discarded). For the observations on September 27, instead of co-adding all maps for the night, we created two maps to allow us to study variations on shorter temporal scales in the hours following the impact. The results are shown in Figure 3. The reflectance slope shown in the maps (hereafter referred to as colour) is expressed in units of %/100 nm. We note that in the analysis below, we do not compare the colour of the central condensation (dominated by Didymos) seen in the maps presented in Figure 3 to that of the ejecta. The reason for this is to avoid any bias due to the difference in PSF size between the short and long wavelength part of the data. This manifests in Figure 3 as a dark annulus (negative reflectance slope) around the central condensation, which is an artefact and not a real feature of the ejecta. To define the reflectance of the system pre-impact and to avoid this effect, we used spectra extracted over the full PSF of the object from observations on September 26, rather than using colour maps. In some parts of Figure 3, a check-like pattern can be seen in the colour maps. This pattern is due to the combination of design of MUSE which is composed of 24 different detectors (creating a rectangular pattern) and the observing strategy (small dithering and 90-degree rotations were applied between each exposure).

We examined the reflectance maps to study the evolution of the ejecta and tail properties over time. In the hours following the impact, on September 27, the initial ejecta cloud is clearly visible in the colour maps with a reflectivity of the order of $0-4$%/100 nm. This is significantly bluer (i.e. with a shallower reflectance slope) than the system before impact, for which we measure a colour of 12%/100 nm. This is also illustrated in Figure 1 that shows that the increase in the relative reflectance with the wavelength is less pronounced after impact. As mentioned above, by 07:00 UT on September 27 the tail is already visible in our data with a reflectivity of $5-7$%/100 nm. This is about a factor of 2 higher than the broader ejecta seen in the first two colour maps. By September 28 (and even more on September 29) the two spirals described in Section 3.2 are visible in the colour maps. On September 29 they have reflectance slopes of the order of $5-9$%/100 nm, similar to the tail on the same date, with the northen spiral slightly bluer than the southern one. On October 3 some material can be seen to the right of the northern feature, of the order of a few %/100 nm bluer than the tail at the same distance from the edge of the northern feature. As time passes the tail becomes redder, from $5-6$%/100 nm on September 27

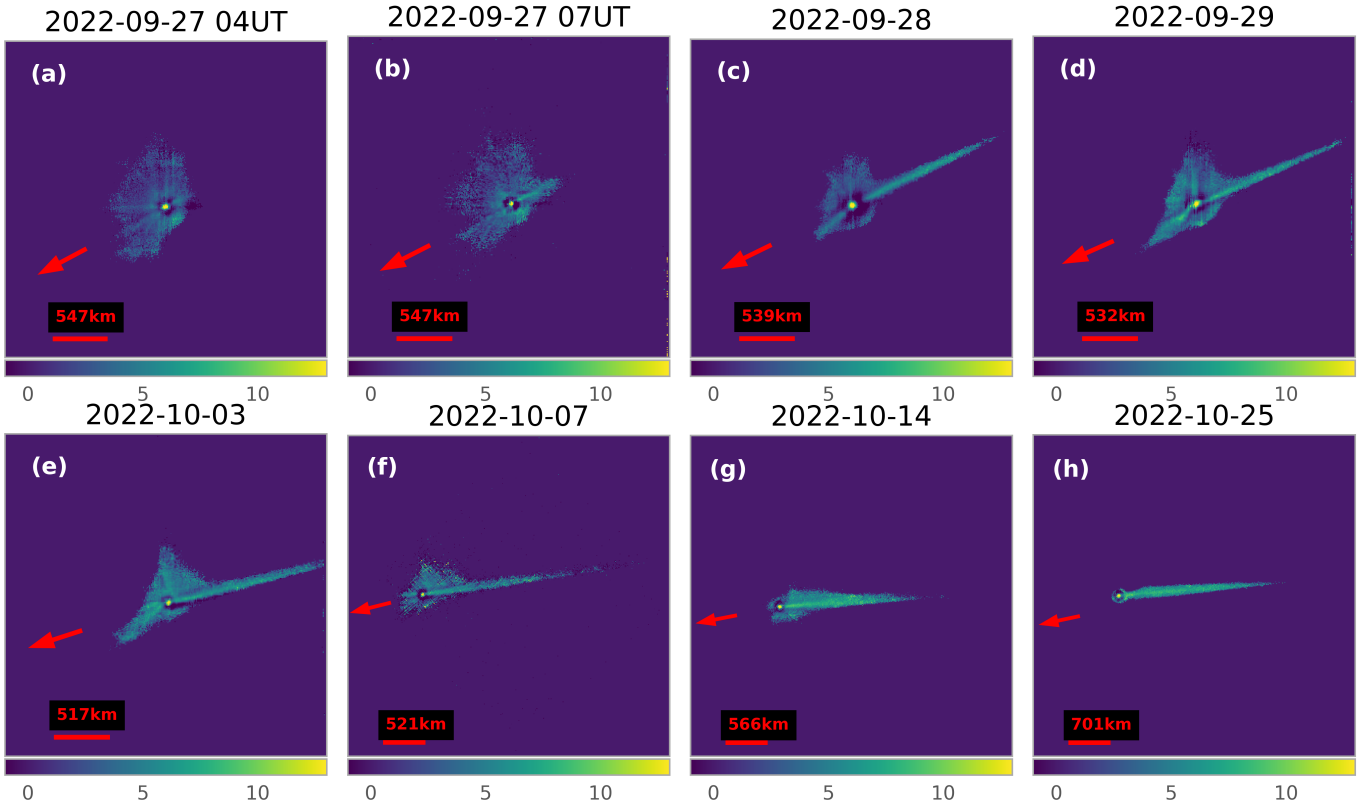

Fig. 3. Maps of the reflectance slope between 500 and 850 nm, normalised at 600 nm for WFM observations. The maps are oriented north up and east left. The direction of the Sun is indicated by a red arrow and a scale bar is shown in each panel. The time above each map is the average time of the stack; the reflectance slope indicated by the colour bar is expressed in units of %/100 nm. A cut-off was applied to mask spaxels with little to no target signal.

to 7 – 10%/100 nm on October 25. Finally, we do not see any significant colour differences between clumps and the rest of the ejecta in the WFM colour maps.

Changes or differences in the reflectance slope of dust particles are commonly observed in the dust surrounding comets and can have several causes, the two main ones being a change in the composition of the particles and a change in their size distribution (Jewitt & Meech 1986). In the case of the particles seen after the DART impact, since the particles ejected come from the same parent body, we assume that the main cause of the colour difference observed is a difference in the particle sizes. As explained below, this is also consistent with the timescale of the different features. In general, bluer dust colours are associated with small particles while redder colours are attributed to larger particles (Jewitt & Meech 1986). We observe that the ejecta is bluer than the tail. This is consistent with the initial ejecta being made of smaller particles, which would leave the FoV relatively fast (in the hours following impact), while the tail is composed of larger particles. Li et al. (2023) determined that when it appears, the tail is likely composed of 1 - 10s μm size particles; by comparing the colour of the ejecta cloud to the colour of the tail, and taking into account that it has mostly cleared within two days after impact, we postulate that the initial ejecta is likely composed of 1 μm – 10s μm sized dust. The tail becomes redder with time as the smaller particles are pushed further by the radiation pressure and leave the FoV of MUSE. In panels (e) and (f) of Figure 3, the feature towards the north is associated with particles from the northern spiral being pushed and spread out by the effect of the solar radiation pressure. This appears slightly bluer than the tail at the same distance from the object, consistent with what would be expected for particles smaller than those of the tail that were first ejected towards the Sun and then turned back by the radiation pressure, as postulated by Li et al. (2023).

4. Conclusions

We analysed observations performed with the MUSE instrument before and up to a month after the DART impact, probing a range of spatial and temporal scales. We used these data to search for gas emission following the impact, study the morphology of the ejecta, and measure its spectral properties. We draw the following conclusions:

- After searching for emission from [OI], Xe, NH_2, or H_2O^+, we do not detect gas around the system in our observations, which started 3h40m after the impact.
- We observe a number of dust morphological features around the system after the impact, including clumps, consistent with what was observed with HST (Li et al. 2023).
- We do not detect strong colour differences between the clumps and the initial ejecta cloud. The tail and the two spirals, however, have a redder colour (steeper reflectance slope) than the initial ejecta. This indicates that the initial ejecta is made of relatively small (and faster moving) parti-

cles leaving the FoV in the hours and days following the impact, while the spirals and tail are made of larger particles. We also see bluer particles to the west of the northern spiral a week after impact, likely smaller particles originally ejected towards the Sun and then accelerated by radiation pressure. Over time, the tail becomes redder, consistent with a particle size selection effect due to the solar radiation pressure.

The IFU nature of the MUSE instrument combined with adaptive optics capabilities allowed us to perform this unique combined analysis of the morphology and spectral properties of the ejecta following the DART impact, down to subarscecond spatial scales.

Acknowledgements. Based on observations collected at the European Southern Observatory under ESO programmes 110.23XL and 109.2361. The authors wish to acknowledge the exceptional level of support provided by support astronomers and Instrument and Telescope Operators at Paranal Observatory. For the purpose of open access, the authors have applied a Creative Commons Attribution (CC BY) licence to any Author Accepted Manuscript version arising from this submission. This work was supported in part by the DART mission, NASA Contract No. NNN06AA01C to JHU/APL. Funding support from the European Union's Horizon 2020 research and innovation programme under grant agreement No 870377 (project NEO-MAPP) is acknowledged.

References

Arsenault, R., Madec, P. Y., Hubin, N., et al. 2008, in Society of Photo-Optical Instrumentation Engineers (SPIE) Conference Series, Vol. 7015, Adaptive Optics Systems, ed. N. Hubin, C. E. Max, & P. L. Wizinowich, 701524
Bacon, R., Accardo, M., Adjali, L., et al. 2010, in Society of Photo-Optical Instrumentation Engineers (SPIE) Conference Series, Vol. 7735, Ground-based and Airborne Instrumentation for Astronomy III, ed. I. S. McLean, S. K. Ramsay, & H. Takami, 773508
Bagnulo, S., Gray, Z., Granvik, M., et al. 2023, ApJ, Accepted
de Léon, J., Opitom, C., Migliorini, A., et al. 2023, A&A, In preparation
Dotto, E., Della Corte, V., Amoroso, M., et al. 2021, Planet. Space Sci., 199, 105185
Jewitt, D. & Meech, K. J. 1986, ApJ, 310, 937
Kiersz, D. A., Green, S. F., Rivkin, A. S., Fitzsimmons, A., & Seccull, T. 2021, in 7th IAA Planetary Defense Conference, 194
Li, J.-Y., Hirabayashi, M., Farnham, T. L., et al. 2023, Nature, Accepted
Meftah, M., Damé, L., Bolsée, D., et al. 2018, A&A, 611, A1
Opitom, C., Guilbert-Lepoutre, A., Besse, S., Yang, B., & Snodgrass, C. 2020, A&A, 644, A143
Rivkin, A. S., Chabot, N. L., Stickle, A. M., et al. 2021, The Planetary Science Journal, 2, 173
Stief, L. J., DeCarlo, V. J., & Mataloni, R. J. 2020, J. Chem. Phys, 46, 592
Ströbele, S., La Penna, P., Arsenault, R., et al. 2012, in Society of Photo-Optical Instrumentation Engineers (SPIE) Conference Series, Vol. 8447, Adaptive Optics Systems III, ed. B. L. Ellerbroek, E. Marchetti, & J.-P. Véran, 844737
Thomas, T. A., Naidu, S. P., Scheirich, P., et al. 2023, Nature, Accepted
Weilbacher, P. M., Palsa, R., Streicher, O., et al. 2020, A&A, 641, A28

Appendix A: Reflectance

We observed two solar analogues with the WFM and NFM modes to allow us to measure the reflectance of the Didymos–Dimorphos system: HD11532 and HD28099. We also tested a reference solar spectrum obtained using the SOLar SPECtrometer (SOLSPEC) instrument of the SOLAR payload on board the International Space Station (ISS) (Meftah et al. 2018), resampled to match the sampling of MUSE. The two solar analogues and solar reference spectrum gave similar results, as illustrated in Fig. A.1, and we decided to use the solar spectrum for this analysis. The reflectance spectrum shown in Fig. A.1 was measured in an aperture of 5″ for the data obtained on September 27, a few hours after impact. Observations were performed simultaneously with the X-Shooter spectrograph on the UT2 at the VLT, using the same solar analogues as those used for the MUSE observations. The reflectance spectrum shape and slopes measured with the same analogue and with a similar aperture with both instruments are consistent with each other (de Léon et al. 2023). The shape of the reflectance spectrum we obtained is also consistent with the reflectance measured by the FORS2 instrument on the VLT at a similar time (Bagnulo et al. 2023). Finally, it has a similar shape to what was measured for the system pre-impact (Kiersz et al. 2021).

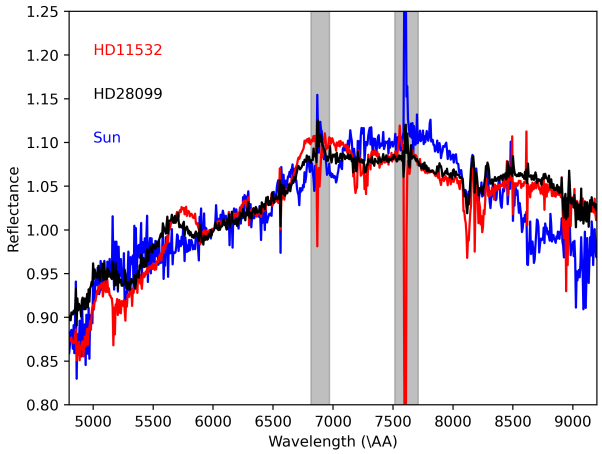

Fig. A.1. Reflectance measured within a 5″ radius aperture on September 27, using a solar spectrum, and two solar analogues (HD28099 and HD11532). Grey areas are strongly affected by telluric absorptions.